Experimental and Numerical Investigation of the Uplift Capacity of Plate Anchors in Geocell-Reinforced Sand

M. Rahimi[1], S.N. Moghaddas Tafreshi[2, *] (Corresponding Author), B. Leshchinsky[3], A.R. Dawson[4]

[1]Department of Civil Engineering, K.N. Toosi University of Technology, Valiasr St., Mirdamad Cr., Tehran, Iran. Tel: +982188779473; Fax: +982188779476; E-mail address: my.rahimi@mail.kntu.ac.ir

[2,]Corresponding Author. Department of Civil Engineering, K.N. Toosi University of Technology, Valiasr St., Mirdamad Cr., Tehran, Iran. Tel: +982188779473; Fax: +982188779476; E-mail address: nas_moghaddas@kntu.ac.ir*

[3]Forest Engineering, Resources and Management Department, College of Forestry, Oregon State University, 280 Peavy Hall, Corvallis, Oregon 97331, USA. Tel: +1541-737-8873; E-mail address: ben.leshchinsky@oregonstate.edu

[4]Nottingham Transportation Engineering Centre, University of Nottingham, Nottingham, UK. Tel: +441159513902; Fax: +441159513909; E-mail address: andrew.dawson@nottingham.ac.uk

Abstract: Plate anchors are frequently used to provide resistance against uplift forces. This paper describes the reinforcing effects of a geocell-reinforced soil layer on uplift behavio~~u~~r of anchor plates. The uplift tests were conducted in a test pit at near full-scale on anchor plates with widths between 150 and 300 mm with embedment depths of 1.5 to 3 times the anchor width for both unreinforced and geocell-reinforced backfill. A single geocell layer with pocket size 110 mm×110 mm and height 100 mm, fabricated from non-perforated and nonwoven geotextile, was used. The results show that the peak and residual uplift capacities of anchor models were highest when the geocell layer over the anchor was used, but with increasing anchor size and embedment depth, the benefit of the geocell reinforcement deceases. Peak loads between 130% and 155% of unreinforced conditions were observed when geocell reinforcement was present. Residual loading increased from 75% to 225% that of the unreinforced scenario. The reinforced anchor system could undergo larger upward displacements before peak loading occurred. These improvements may be attributed to the geocell reinforcement distributing stress to a wider area than the unreinforced case during uplift. The breakout factor increases with embedment depth and decreased with increasing anchor width for both unreinforced and reinforced conditions, the latter yielding larger breakout factors. Calibrated numerical modelling demonstrated favorable agreement with experimental observations, providing insight into detailed behavior of the system. For example, surface heave decreased by over 80% when geocell was present because of a much more efficient stress distribution imparted by the presence of the geocell layer.

Keywords: *Geosynthetics, Plate anchor, Geocell layer, Uplift load, Upward displacements, Numerical analysis*

Formatted: Not Highlight

1. Introduction

In recent years, geosynthetics have become increasingly common due to their cost-efficiency in reinforcement applications. Geosynthetics are commonly manufactured in planar form (geotextiles, geogrids, geonets, geomembranes, strips), but three-dimensional (3D) reinforcements, such as geocells, are increasingly being adopted for soil reinforcement applications (Koerner, 2012). Geocells have demonstrated particular utility for foundation support, embankment protection, subgrade stabilization and earth retention (e.g. Tanyu et al., 2013; Moghaddas Tafreshi et al., 2013; Hegde and Sitharam, 2015; Biabani et al., 2016) but there is limited research towards assessing the efficacy of geocells towards increasing uplift resistance of earth anchors (e.g. Choudhary and Dash, 2013, Moghaddas Tafreshi et al., 2014). There is promise in such an application, however, as geocells increase soil strength by confinement, reducing lateral displacement and causing the confined composite to act as a stiffer mattress-like composite (Zhang et al., 2010).

Various structures are subject to loading that require the uplift resistance of anchors, including free-standing towers, wind turbines, submerged pipelines, chimneys, suspension bridges, and roofs (Ilamparuthi et al., 2002). In these applications, anchors are commonly embedded within nearby soil to provide stability and transmit tensile forces to a competent medium (Krishnaswamy and Parashar, 1994; Ghosh and Bera, 2010; Rangari et al., 2013). Anchors are the typical means of resisting these loads, commonly found in the form of plate anchors, helical anchors, deadman anchors, pile anchors, and drag anchors (Sabatini et al., 1999). The uplift capacity of a buried anchor typically comprises of the weight of soil within the failure zone as well as frictional and/or cohesive resistance along the realized failure surface. The required uplift capacity of these systems can be enhanced by increasing the size and embedment depth of the anchor or improving backfill strength and density (Choudhury and Subba Rao, 2005; Kumar and Bhoi, 2009; Song et al., 2009; Vishwas and Kumar, 2011; Liu et al., 2012; Wang and O'Loughlin, 2014; Tian et a., 2014; Bhattacharya and Kumar, 2014, 2015; Ganesh and Sahoo, 2016; Khan et al., 2017; Moayedi and Mosallanezhad, 2017; Shin et al., 2016).

Extensive research has been performed to improve assessment of anchor uplift behavior within unreinforced soil, comprising of experimental, analytical and numerical studies. Early research on anchor uplift capacity was performed under 1G conditions in the context of stabilizing transmission towers and was primarily limited to scaled laboratory experiments to demonstrate the effects of shape, embedment, soil conditions and soil types on anchor resistance (Meyerhof and Adams, 1968; Das and Seeley, 1975; Murray and Geddes, 1987; Frydman and Shaham, 1989; Ilamparuthi et al., 2002; Merifield and sloan, 2006; Sakai and Tanaka, 2007; Song et al., 2008; Kouzer and Kumar, 2009; Khatri and Kumar, 2009; Deskmukh et al., 2010; Horpibulsuk and

Niramitkorburee, 2010; Honda et al., 2011). To better capture realistic, scaled gravitational conditions, centrifuge-based laboratory experiments have been employed in assessing uplift capacity (Dickin, 1988; Tagaya et al., 1988; Dickin and Leung, 1990). Theoretical uplift solutions have been developed by using cavity expansion theory (Vesic 1971), limit equilibrium theory (Meyerhof and Adams, 1968, Murray and Geddes, 1987, Ghaly and Hanna, 1994; Sahoo and Khuntia, 2017), reverse hopper theory (Lee et al. 2014), and elasto-plastic continuum analyses (Rowe and Davis, 1982, Tagaya et al., 1988). However, there is very little research studying the effect of geosynthetic reinforcement in realizing uplift capacity. Extensive experimental research has been performed on assessing the mechanism and uplift capacity of plate anchors in dry, cohesionless sand. Dickin (1988) investigated the uplift behavior of square plate anchors through use of a centrifuge and 1G experiments, demonstrating that anchor geometry has a notable influence on the breakout factor and failure mechanism. In consideration of possibly ~~unconservative~~ non-conservative scale effects, Dickin (1988) proposed an alternative set of breakout factors derived from Meyerhof and Adams (1968) and Murray and Geddes (1987) for different plate sizes with similar embedment ratios. The solution demonstrates good agreement with the experiments, but overestimates the small scale centrifuge results for embedment ratios (i.e. depth of embedment, *D*, divided by anchor width, *B*) exceeding $D/B > 4$.

Employing large or deeply embedded anchors may not always be economical or practical means of obtaining the required anchor capacity. An alternative approach is to use smaller and/or less embedded anchors beneath geosynthetic reinforcements (Krishnaswamy and Parashar, 1994; Ilamparuthi and Dickin, 2001, Ghosh and Bera, 2010; Keskin, 2015). There is some insight into the load-bearing behavior of soil reinforced by geogrids and geotextiles (Binquet and Lee, 1975; Yetimoglu et al, 1994; Karpurapu and Bathurst, 1995; Dash et al, 2003; Moghaddas Tafreshi and Rahimi, 2012; Tran et al., 2013; Vahedifard et al., 2016; Ouria and Mahmoudi, 2018, Dawson and Lee, 1988; Jones et al, 1991). Three-dimensional cellular reinforcement has also been employed in this way (Yoon et al., 2008; Leshchinsky and Ling, 2013; Moghaddas Tafreshi et al., 2014; Hegde and Sitharam, 2015; Guo et al., 2015; Indraratna et al., 2015; Biabani et al., 2016; Trung Ngo et al., 2016; Moghaddas Tafreshi et al., 2016; Oliaei and Kouzegaran, 2017; Song et al., 2017). However, there is limited research improved anchor uplift capacity from geosynthetics - and that is almost entirely limited to the use of planar inclusions, such as geotextiles and geogrids, in dry sand. Krishnaswamy and Parashar (1994) investigated the uplift capacity of small-scale anchor plate embedded in dry sand with and without geosynthetics, finding that reinforcement can increase uplift capacity significantly. Ilamparuthi and Dickin (2001) investigated the behavior of small-scale belled piles embedded in sand, finding increased uplift

Field Code Changed

Field Code Changed

resistance when reinforced with geogrids and geocells. Ghosh and Bera (2010) reported the results of experimental investigations on the effect of geotextile ties on uplift capacity of anchors embedded in sand.

Probably, use of geosynthetics with anchors will only be a practical and economic technique when the soil is compacted in layers after the anchor has been placed. Such use is likely to be less suitable when an anchor is to be installed in pre-existing soil strata as, otherwise, excavation and replacement of the covering soil would then be needed. In these latter circumstances, granular pile anchor foundations (GPAFs) may be used (Kumar and Rao (2000); Phani Kumar et alr (2004)). These comprise an anchor plate, placed at the bottom of a hole that is backfilled with granular soil, connected by cable or rod to foundation above. These GPAFs~~Granular pile anchors~~ are frequently used in expansive soils to resist the uplift forces mobilized ~~in the foundations~~ due to the swelling behaviour of soils. Kumar and Rao (2000) and Rao and Phanikumar (2000) established that the pullout capacity of such granular pile anchors is~~are~~ increased ~~from the presence of base~~when geosynthetics are used at the base, above the anchor plate, mainly owing to increased frictional resistance between the reinforcement and the confining medium. ~~kumar~~ Kumar (2016) similarly reported that geogrid reinforcement increases the uplift capacity of granular pile-anchor in expansive clay beds. Choudhary and Dash (2013) and Moghaddas Tafreshi et al. (2014) studied the effects of geocell reinforcement on enhancing the uplift capacity of anchors and belled piles, both demonstrating significant improvement when the reinforcement was present. However, there is limited analysis of anchor behavior in geocell-reinforced backfill and extrapolation to geometric configurations. Thus, this study expands on prior contributions by introducing the results of a comprehensive testing program on near full-scale anchors performed on a laboratory pit in unreinforced- and geocell-reinforced backfill.

2. Experimental Series

A series of near full-scale tests (a total of 22 independent tests plus 28 repeated tests) on horizontal square plate anchor installed in unreinforced soil and geocell-reinforced soil was performed to:

a) evaluate the influence of geocell confinement above plate anchors subject to uplift loading,

b) investigate the influence of embedment depth and plate size on uplift capacity, and

c) ~~and~~ calibrate numerical analyses that simulate the uplift response of the plate anchor and provide insight into internal behavior of both the geocell and backfill.

Only one type of geocell, one height (h) and pocket size (d) of geocell, and one type of soil were used in this study. Thus, d/B and h/B ratios adopted might not be the optimum values and a change in d/B and h/B might change the results. Other soils might change the benefit and/or the optimum geometrical arrangements.

Commented [K1]: Dear Andrew: could u mix the works of Kumar and Rao (2000) and kumar (2016)? (See references id needs)

Formatted: Not Highlight

Formatted: Not Highlight

Nonetheless, the results still inform general trends that may be expected from use of geocell reinforcement in anchoring applications.

3. Test Materials

3.1. Soil Properties

The soil for both backfill and infill used in the experimental series was consistent throughout all of the physical experiments – well-graded sand (*SW* in the Unified Soil Classification System, ASTM D 2487-11, G_s=2.66). There is a significant quantity of fine gravel (46%) and little fines (<1%), as shown in the grain size distribution (**Fig. 1**). From modified proctor compaction testing (ASTM D 1557-12), the maximum dry unit weight of this soil was determined about 20.42 kN/m^3 with an optimum moisture content of approximately 5.1%. The angle of internal friction (ϕ) of the soil, obtained by consolidated undrained triaxial compression tests at a wet density of 19.72 kN/m^3 (92% relative compaction with moisture content of 5%, similar to the compacted density of the backfill soil layers - see Table 2) of specimens was 40.5°.

3.2. Geocell Properties

The geocell used in the tests had a pocket size (*d*) and height (*h*) of 110 mm ×110 mm and 100 mm, respectively. **Fig. 2** shows an isometric view of the geocell placed over the bottom soil layer and plate anchor. The geocell used in testing was fabricated from a type of a non-woven polymeric geotextile that was thermo-welded to form a 'non-perforated geocell'. The engineering properties of this geotextile, as listed by the manufacturer, are presented in **Table 1**. According to the manufacturer (Treff, 2011), the tensile strength and stiffness of the geocell joint is higher than, or similar to, that of the geocell wall material (i.e. geotextile) preventing seam rupture (Moghaddas Tafreshi and Dawson, 2012).

4. Test Pit and Loading System

4.1. Test Pit

Testing was performed in an vertical indoor test pit, measuring 2200 mm × 2200 mm in plan and 1000 mm in depth, wherein the soil, anchor, geocell layer and instrumentation (i.e. load cell, LVDT and pressure cells) was installed (see **Fig. 3**). As the width and depth of the test pit were respectively more than seven and three times bigger than the maximum width of the anchor dimensions (B =150, 225 and 300 mm), the boundary effects were not considered significant (Consoli et al., 2012a; b). During anchor uplift, it was observed that the surface heave above the anchor was less than three times of the anchor width, corroborating the aforementioned assumption. **Fig. 3a** illustrates a photograph of equipment installation prior to loading. A typical schematic of the test set-up is shown in **Fig. 3b**.

4.2. Loading and Data Acquisition Systems

The loading system (**Fig. 3**) included a loading frame, hydraulic actuator, and a controlling unit. The frame consisted of two heavy steel columns fixed into a strong floor and spanning the width of the test pit, supporting the hydraulic actuator. The hydraulic actuator and control unit may produce monotonic or repeated loading with the capability of applying a stepwise, controlled load with a maximum capacity of 100 kN. The data acquisition system recorded uplift load, upward displacement and in-situ soil pressure. A S-shaped load cell with the accuracy of ±0.01% for a full-scale capacity of 100 kN was placed between the loading shaft and a rod attached to the plate anchor (see **Fig. 3**). A stiff 40 mm diameter rod was employed so that the deflection measured externally would be sensibly the same as that of the plate anchor. To measure the displacement of the plate anchor during the loading, a linear variable differential transducer (*LVDT*) with the accuracy of 0.01% of full range (100 mm) was attached to the loading shaft and the supporting beam as shown in **Fig. 3**. Vertical stress within the backfill was monitored with two soil pressure cells (abbreviated to SPC, 50 mm diameter with an accuracy of 0.01% of full range of 1000 kPa). The left and right soil pressure cells (abbreviated to "L.SPC" and "R.SPC", respectively) are located at 40 and 200 mm away from the center of anchor, approximately at a depth of 100 mm above the anchor (**Fig. 3b)** for both unreinforced and geocell-reinforced tests. To ensure an accurate reading, all of the devices were calibrated prior to each test series.

4.3. Preparation of Test Pit and Experimental Procedure

In order to ensure consistent soil density within the test pit, both unreinforced and geocell-reinforced soils were compacted with a handheld vibrating plate compactor, 450 mm in width. According to the embedment depth of anchor, the unreinforced soil layers were prepared and compacted at thicknesses of either 50, 75 or 100 mm with, respectively, one, two or three passes of compactor to achieve the required density (i.e. dry unit weight of ≈18.76 kN/m^3 in **Table 2**). To achieve the required density of soil in the pockets of the geocell layer (shown in **Table 2)**, it was compacted with four passes of compactor. This amount of compactive effort was maintained throughout all tests. The depth of influence of the compactor is specified as 50-100 mm, diffusing any added compaction in deeper layers. Sand cone tests (ASTM D1556-07) were conducted to measure the densities of compacted soil and geocell infill, ensuring compliance to a relative compaction levels that remained within 91-93% (average moisture content between 4.8% and 5.2%). **Table 2** shows the average measured dry unit weights of unreinforced soil and geocell infill after compaction of each layers. The anchor plate, with the rod of desired length attached, was placed in the center of the test pit on the compacted soil layer surface after the first 100mm of soil was placed. Thereafter, the geocell reinforcement panel was extended above the anchor.

The cell pockets were filled with backfill soil to include about 10 mm thickness of extra soil over the geocell, after which compaction of infilled was continued until appropriate density was achieved. Thereafter, two soil pressure cells were installed (see **Fig. 3b**) and the load cell was connected between the actuator and plate anchor along with an LVDT. When the system was ready for testing, tensile uplift loading was applied monotonically at an equivalent pressure increase of 1.5 kPa per second while upward displacement, uplift force and soil pressure were monitored and recorded using LVDT, load cell and soil pressure cells (“L.SPC” and “R.SPC”), respectively. Testing was stopped when failure (a peak load) was observed. In the absence of a distinct failure peak, the uplift was stopped at an upward displacement of 20 mm.

5. Testing Program

The geometry of the test configurations for the anchor plate embedded in unreinforced and geocell-reinforced backfill is as shown in **Fig. 3b**. Three sizes of steel anchor plates (B=150, 225, 300 mm, 25.4 mm in thickness) with four embedment depth ratios (D/B=1.5, 2, 2.5, 3) in both unreinforced and geocell-reinforced backfill were examined under static loads (**Table 3**). Choudhary and Dash (2013) discussed that geocell width may influence the performance of plate anchors, observing decreasing gains in improvement of uplift carrying capacity when geocell width increasing beyond 2 times the anchor width (b=2B). Thus, to achieve the maximum performance of geocell reinforcement, the width of the geocell layer (dimension b) was selected to be approximately three times the plate width ($b/B \approx 3$)~~,~~ – i.e. with ~~the~~ geocell widths of about 450 mm, 675 mm and 900 mm, respectively for anchor widths of 150 mm, 225 mm and 300 mm. The thickness of the geocell layer above the anchor plate was held constant in all the tests at 100 mm. Several replicate tests were performed for each configuration ~~for~~ so as to give confidence in the experimental results and anchor behavior. Anchor capacities determined for a given test configuration never demonstrated more than 8% difference indicating that the test results were, effectively, repeatable ~~reliable~~.

6. Experimental results

In this section, the results of the uplift tests are presented along with a discussion highlighting the effects of the anchor embedment depth, anchor width, and geocell reinforcement on uplift capacity and the pressure above the anchor.

6.1. Behavior of Unreinforced and Reinforced Beds

The monotonic uplift load-displacement relationship of unreinforced and geocell-reinforced systems are shown in **Fig. 4**. For all unreinforced anchor systems, the general trend of uplift load with displacement is consistent although there are key differences between the reinforced and unreinforced system’s responses.

Commented [K2]: Dear Andrew: is the edit ok?

Formatted: Not Highlight

Formatted: Not Highlight

When unreinforced, a distinct peak uplift load was observed at an outward displacement equal to 2-6 mm, and thereafter there is a significant reduction until a sustained residual load is reached. In contrast, the geocell-reinforced system demonstrates sustained uplift resistance after a peak load occurring at displacements between 5-11 mm. No clear post-peak reduction in load capacity is observed for these cases. At a given imposed load level, the anchor embedded in a geocell-reinforced soil had a smaller outward displacement than the anchor embedded in the equivalent unreinforced bed. Soil reinforced with geocell had a higher initial stiffness and strength and ductility than an untreated system. **Fig. 4** also shows that both the peak and the residual uplift load increased with anchor width and embedment depth for both unreinforced and reinforced conditions. Peak reinforcement loads are about 40% higher than the equivalent unreinforced peak loads.

In general, the uplift load-displacement response of unreinforced and reinforced systems are shown in **Fig. 5**. A three-stage behavio~~u~~r illustrated in **Fig. 5a**, is observed in uplift tests on unreinforced system. They are:

Stage 1) Pre-peak behavio~~u~~r: the uplift load rises rapidly with the displacement towards a peak value (P_{peak}).

Stage 2) Post-peak behavio~~u~~r: rapid reduction in the pullout load occurs as displacement occurs.

Stage 3) Residual behavio~~u~~r: final, unchanging residual/sustained uplift load ($P_{res.}$) at large displacements. For the unreinforced response, a significant difference between peak and residual upward displacement is evident.

For the geocell-reinforced system, two-stage behavio~~u~~r is mostly observed as shown in **Fig. 5b**. The observed stages are:

Stage 1) Pre-peak behavio~~u~~r: a rapid increase in uplift load with the displacement.

Stage 2) Post-peak behavio~~u~~r: insignificant reduction from peak load (P_{peak}) to a residual load ($P_{res.}$) which remains close to the peak uplift load.

The three-phase behavio~~u~~r of unreinforced system is similar to the load-deflection behavior of dense ~~bed~~ sand where material dilation under shear means that significant energy and displacement is needed to rearrange particles into a fabric that can shear, after which much less energy is needed to continue the shearing. Hence the residual strength is considerably less than the peak value. It is also similar to the response seen (in compression) beneath shallow foundations undergoing 'general' failure, as defined by Vesic (1963). The low confinement allows dilation to take place so that, once peak bearing capacity is reached, subsequent deflection requires less load. (or shallow anchors) ~~whereas~~

In contrast, the two-phase behavior of reinforced system is similar to the behavior of a medium dense sand ~~bed~~where the fabric allows peak strength to be reached without dilation (so there is no post-peak load reduction

Formatted: Not Highlight

as deformation continues), or in contained punching failure (Vesic, 1963) where the surrounding stress prevents dilation ~~(or deep anchors)~~.

This it appears that, at least in the arrangements tested here, the reinforced systems prevented dilation around the anchor and, thus, lead to a response without a post-peak load capacity reduction. The geocell layer thus performs a potentially critical role in providing a more reliable load capacity should large deflections occur.

6.2. Uplift Capacity and Upward Displacement of Anchor

The variation of peak and residual uplift loads of anchors as a function of embedment depth are presented in **Figs. 6a** and **6b** for unreinforced and reinforced systems respectively. Both peak and residual uplift loads of unreinforced and reinforced beds increase approximately linearly with anchor embedment depth. For instance, an anchor width of 300 mm in reinforced soil showed peak uplift loads for embedment depth of 1.5, 2, 2.5 and 3.0 of 8.88, 14.57, 20.54 and 25.74 kN, respectively. For these tests, the corresponding uplift displacements were found to be about 5-11 mm (**Fig. 4c** and **Table 4**).

This figure also demonstrates that for the larger widths (B=225 and 300 mm) of anchor, the variation of both the peak and residual uplift loads with embedment depth is significant wh~~ere~~ile it is ~~not~~ insignificant for the smallest width (B=150 mm) of anchor. It may be noted that small-scale models may not always give reliable assessments but, more significantly, that if large-scale models or full-size plate anchors are allowed to be displaced they can generate significant load capacities – especially if the latter is covered in a geocell-reinforced soil layer. **Fig. 6** also shows that the values of both peak and residual uplift loads increase with anchor width, irrespective of embedment depth (ratio of D/B). The rate of increase in peak uplift capacity with anchor width between 225 and 300 mm was about 1.75 times that for anchor widths between 150 and 225 mm.

Formatted: Not Highlight
Formatted: English (United States), Not Highlight
Formatted: Not Highlight
Formatted: English (United States), Not Highlight
Formatted: Not Highlight
Formatted: English (United States), Not Highlight

For the purpose of this paper, the improvement in peak and residual uplift loads due to the presence of geocell reinforcement are represented using two non-dimensional improvement factors:

(1) Improvement in peak uplift load of anchor (IF_{peak}) which compares the peak uplift load of the geocell-reinforced system to that of the unreinforced system, defined as:

$$IF_{peak} = \frac{(P_{peak})_{rein.}}{(P_{peak})_{unrein.}} \quad (1)$$

Field Code Changed

(2) Improvement in residual uplift load of anchor ($IF_{res.}$) of the geocell-reinforced system to that of the unreinforced system, defined as:

$$IF_{res.} = \frac{(P_{res.})_{rein.}}{(P_{res.})_{unrein.}} \quad (2)$$

Field Code Changed

where $(P_{peak})_{rein.}$ and $(P_{peak})_{unrein.}$ are the values of peak uplift load of the geocell-reinforced and unreinforced systems, respectively and $(P_{res.})_{rein.}$ and $(P_{res.})_{unrein.}$ are the values of residual uplift load of the geocell-reinforced and unreinforced systems corresponding to 20 mm of upward displacement of anchor, respectively. It should be noted that, if the anchor embedded in unreinforced or geocell-reinforced system reaches its residual uplift capacity at a displacement larger than 20 mm (not shown in **Fig. 4**), the residual uplift capacity at 20 mm upward displacement was taken as the residual value.

Together, **Figs. 4** and **Figs. 6** show that geocell reinforcement exhibits increased load capacity at all embedments, all displacements and all anchor widths when compared to the corresponding unreinforced geometry. The variation of value of the improvement factors (IF_{peak} and $IF_{res.}$) are shown for varying anchor embedments and widths in **Fig. 7a**. Generally, the improvement in residual uplift load ($IF_{res.}$) - i.e. the reinforcing efficacy - decreases with increase in the embedment depth and anchor width. Moreover, the results show that despite a significant decrease in $IF_{res.}$ with increase in embedment depth and anchor width; however, the variation of IF_{peak} between tests is not significant. It can be also seen that IF_{res} values are larger than the values of IF_{peak}, irrespective of the embedment depth and anchor width. Hence, beneficial effect of geocell is more pronounced when the design of anchor plate is based on the residual uplift capacity of anchor.

Fig. 7b depicts the variation of $P_{res.}/P_{peak}$ with embedment depth of anchor (D/B) for different anchor widths. It shows that the use of geocell reinforcement leads to stabilizing post-peak behavior with a maximum reduction of less than 10% from the peak load to a residual load ($P_{res.}/P_{peak}$>90%), whereas unreinforced installations demonstrate more than a 45-55% reduction from peak load to the residual for anchor widths of 150 and 225 mm and about 20-40% for an anchor widths of 300 mm. The differences in IF values and in P_{res}/P_{peak} (**Fig. 7b**) ratios for reinforced conditions are attributable to the geocell layer preventing narrower, localized shear failure within the overburden soil. Generally, geocell reinforcement provide a stronger, more ductile anchoring system than unreinforced plate anchors. This behavior is attributable to wider mobilization of soil shear strength and overburden as well as added tensile resistance of the geocell mattress. The slab-like behavior of the geocell provides higher residual uplift resistance. Similar observations have been made for uplift resistance of reinforced, small scale belled piles (Ilamparuthi and Dickin 2001 and Moghaddas Tafreshi et al. 2014).

Table 4 shows the upward displacement at peak uplift resistance (abbreviated to u_{peak}) for both unreinforced and reinforced systems. For a given embedment depth and anchor width of, u_{peak} is greater in the reinforced system compared to that in unreinforced system. However, it should be noted that use of geocell reinforcement provides significantly larger resistance than the unreinforced case at moderately small displacements (i.e. 1-5mm). Generally, the unreinforced and reinforced systems provided a similar load-displacement response at small displacements (i.e. 0-2 mm) as geosynthetic reinforcement requires strain or displacement to mobilize resistance. The results in **Table 4** also reveal that for both unreinforced and geocell-reinforced systems, u_{peak} increases with embedment depth and anchor width, attributable to increased overburden resistance. To make direct comparisons of the upward displacement of anchors in reinforced and unreinforced systems, a non-dimensional parameter of $(Iu)_{peak}$ is defined as:

$$(Iu)_{peak} = \frac{(u_{peak})_{rein.}}{(u_{peak})_{unrein.}} \qquad (3)$$

Field Code Changed

where $(u_{peak})_{rein.}$ is the displacement corresponding to the peak uplift load in the reinforced system, and $(u_{peak})_{unrein.}$ that of the unreinforced systems. $(Iu)_{peak}$ decreases with increase in the embedment depth of anchor for all anchor widths (e.g. from 2.79 to 1.98 as embedment depth increases from 1B to 3B for the 225 mm wide anchor, **Table 4**). $(Iu)_{peak}$ also decreases with increasing anchor width for all the embedments (e.g. from 4.03 to 1.56 as anchor width increases from 150 mm to 300 mm, for the 2.5B embedment). This may be attributable to the load dispersion geometry occurring due to shear transfer in the geocell system. This would suggest that geocell reinforcement would be most efficient when placed perpendicular and nearby to the reinforcement layer. That is, reinforcement is most effective when a concentrated loading occurs close to a geosynthetic system as it provides maximum interaction, ~~greater~~ provides localized resistance to shear displacements~~,~~ and increased load ~~dispersion~~ speading – an observation made for reinforced foundation systems (Binquet and Lee, 1975; Dawson and Lee, 1988; Yetimoglu et al, 1994; Karpurapu and Bathurst, 1995; Dash et al, 2003; Moghaddas Tafreshi and Dawson, 2012; Thakur et al., 2012; Tran et al., 2013; Moghaddas Tafreshi et al., 2013). Similarly, mobilization of reinforcement loading tends to be restricted to only part of a flexible geosynthetic system; hence, the extent of the reinforcement geometry should be considered in design.

6.3. Breakout Factors

The *breakout factor* (N_q) is commonly used to define uplift capacity (Bowles, 1996; Goel et al., 2006). The breakout factor is defined from the results of tests, in a dimensionless form as:

$$N_q = \frac{P_{peak}}{W} = \frac{P_{peak}}{\gamma AD} \quad (4)$$

Field Code Changed

Where N_q is anchor breakout factor, P_{peak} is the anchor ultimate uplift capacity, W is the soil weight above the anchor, γ is the unit weight of soil, D is the embedment depth of the anchor and A is the anchor area which in this paper defines as B^2 for a square anchor. **Fig. 8** shows breakout factors as a function of embedment depth and anchor width of anchor for both unreinforced and geocell-reinforced systems. This figure shows that the breakout factor increases with embedment depth and decreases with increase in the width of anchor, whether unreinforced or reinforced, agreeing with the findings of Ravichandran et al. (2008). For all embedment depths and widths of anchor, the geocell-reinforced system delivers a larger breakout factor than unreinforced conditions.

6.4. Soil Pressures over the Anchor

In order to demonstrate how geocell reinforcement distributes uplift pressures, the variation of measured stress with upward displacement of anchor is plotted in **Fig. 9** for an anchor width of 300 mm and an embedment depth of 2.5 and 3 (D/B=2.5 and 3) for both unreinforced and geocell-reinforced systems. The stress plotted is that inside the soil medium at a point 100 mm above the anchor plate, 40 and 200 mm away from the center of anchor (i.e. at the location of the pressure cells “L.SPC” and “R.SPC”) demonstrated in **Fig. 9**. The pressure readings demonstrate that vertical pressure increases with upward anchor displacement. The pressure measured by the left soil pressure cell (“L.SPC”), 40 mm away from the center of anchor, shows a greater pressure increase compared to that of the right pressure cell anchor (“R.SPC”), 200 mm away from the center of anchor. The ratio of the measured maximum pressure by “R.SPC” to that measured by “L.SPC” is about 0.6-0.7 for both unreinforced and geocell-reinforced system, irrespective of embedment depth. The pressure measured 100 mm above the anchor plate is significantly less in the geocell-reinforced system than in the unreinforced system. For example, for the anchor embedded at a depth of 3B, the maximum pressure recorded by “L.SPC”, is 182.4 and 134.4 kPa and by “R.SPC” is 106.4 and 95.2 kPa, for unreinforced and the geocell-reinforced system respectively – reductions of 26% and 10.5%, respectively.

To more clearly demonstrate the effect of geocell reinforcement on uplift pressure dispersion, the soil pressures measured by “L.SPC” and “R.SPC”, corresponding to the peak load obtained in the unreinforced system for the anchor width of 300 mm, are shown in **Table 5.** The maximum uplift pressure in **Table 5** was calculated by dividing the maximum uplift load by the area of the anchor plate. To evaluate the ratio, P, of soil pressure in the reinforced system to that in the unreinforced system, two specific ratios are introduced:

$$P_L = \frac{(L.SPC)_{rein.}}{(L.SPC)_{unrein.}} \tag{5}$$

$$P_R = \frac{(R.SPC)_{rein.}}{(R.SPC)_{unrein.}} \tag{6}$$

In which $(L.SPC)_{rein.}$ and $(L.SPC)_{unrein.}$ are the pressures measured in the reinforced and unreinforced systems, respectively, by the left pressure cells (Eq. 5); while Eq. 6 takes the same approach for the right pressure cell readings. In all cases the values of soil pressure are those measured when the anchor force equals the maximum obtained in the corresponding unreinforced installation. In this way, P_L and P_R values less than unity (as given in **Table 5**) indirectly show how the same anchor force must act over a larger area of soil when geocell reinforcement is present – delivering a stress reduction of between 25% and 41%. This implies a wider tributary area of overburden soil mobilized for uplift resistance. In order to assess these tributary areas, a simple analysis that defined average pressures above the anchor plate ($\sigma_{un.}$ and $\sigma_{re.}$ for unreinforced and reinforced soil, respectively) was used, defined as:

$$\sigma_{re.} = \sigma_{\max} \times \frac{B^2}{B_{re.}^2} \quad \& \quad \sigma_{un.} = \sigma_{\max} \times \frac{B^2}{B_{un.}^2} \tag{7}$$

Where $\sigma_{max}=(P_{peak})_{un}/B^2$ and $B_{re.}$ and $B_{un.}$ are the dimension of back-calculated reinforced and unreinforced tributary area 100 mm above the anchor, defined by a relationship between the dispersion angle, α_{re} and α_{un}:

$$B_{re.} = B + 2h\tan\alpha_{re.} \quad \& \quad B_{un.} = B + 2h\tan\alpha_{un.} \tag{8}$$

Where the parameter h is the height of geocell layer (100 mm in this case). According to the soil pressure results given in **Table 5** for anchor width of 300 mm and Eq. (7), the average value of $B_{un.}$ and $B_{re.}$ for unreinforced and reinforced systems can be calculated as, respectively, about 370 mm and 460 mm. Hence, the mean value of pressure distribution angle, $\alpha_{un.}$ and $\alpha_{re.}$ for unreinforced and reinforced systems respectively, was calculated using Eq. (8) as about 19.3 and 24.7 degrees, respectively. This demonstrates enhanced stress dispersion provided by geocell reinforcement. These results do not directly reveal the mechanism by which this more effective load-distribution is achieved but it may be inferred that the cellular structure confines cell infill and mobilizes greater soil area (Thakur et al., 2012; Moghaddas Tafreshi et al. 2014). Other authors have also attributed this to improved anchorage (Thakur et al., 2012; Tavakoli et al., 2012) so that frictional, "blanketing" effect is achieved by the geocell-soil reinforced layer. Numerical modeling provides better insight into these internal mechanisms that are difficult to observe in physical experiments.

7. Numerical Analysis

Numerical studies serve as a cost-effective means of building upon experimental results without the added expense and labor required for large-scale testing. There is extensive research using numerical techniques to assess unreinforced soil resistance (Merifield and Sloan, 2006; Dickin and Laman, 2007), but to the authors' knowledge, there is no numerical study on uplift capacity of reinforced soil. Furthermore, there is limited research into the complex 3D stress conditions and failure mechanisms associated with buried anchors and geosynthetic inclusions. To better characterize these internal mechanisms, finite element (FE) modeling was performed using a three-dimensional model of soil and geocell based on the large-scale experimental results.

7.1. Finite Element Analysis

Similar to the experiments, only one layer of geocell of fixed aperture width and cell height was modeled. Simulations were performed on three different plate sizes (B=150, 225, 300 mm), four embedment depth ratios (D/B=1.5 to 3) and one reinforcement width to plate anchor width ratio (b/B=3). For this study, twenty-two simulations were performed, consisting of both unreinforced and reinforced cases. For direct comparison with experimental results, 20 mm of upward, vertical displacement was applied rigidly at a location representative of the anchor plate. The computed load was used to evaluate the uplift capacity. The analysis was run in two phases – first a gravity stage where gravity was slowly applied over 100 seconds of virtual time and a loading stage where 20 mm of displacement was imposed over a virtual 1000 second timeframe. Thus, upward movement was applied under displacement control conditions at a rate of 1.2 mm/min (=20 mm/1000 sec.). Over these periods, stresses, displacements, strains and reaction forces were output through use of ABAQUS version 6.12 Explicit, a solver used to analyze large deformation geotechnical problems. Load control conditions may be used in FE modeling, but can lead to numerical difficulties when a user is attempting to determine the ultimate limit state conditions.

Fig. 10a shows the analyzed configurations where D, B and b are as previously defined (see **Fig. 3**). Since the anchor, geocell and the loading were symmetrical, the model replicated only half the physical test arrangements for reduced computational expense as shown in **Fig. 10a**. All points on the vertical x-z plane passing through the center of the anchor plate were constrained from lateral displacement in the y-direction and from rotation around x and z axes (**Figs. 10a)**. **Fig. 10a** also shows the other boundary conditions used. All the vertical, external walls could displace vertically, but not horizontally. The base of the model was restricted from downward displacement during the application of the gravity step, but could translate vertically with any uplift movements. This boundary contains a plate-sized gap in the center of the model (**Fig. 10a**). This gap, with a thickness of 25.4 mm, was the location where displacement boundary conditions of 20 mm were applied during the loading stage and reaction forces were extracted concurrently. The geocell inclusion was placed within the soil using *Embedded Region* conditions in ABAQUS, which mitigates the challenges of mesh congruence at the expense of treating the geocell as a tied material - the case in other numerical studies (Leshchinsky and Ling, 2013). The *Embedded Region* constraint is essentially a tie constraint that determines the spatial relationship of nodes of a given embedded shell/membrane/surface element (i.e. the geocell) with respect to the nodes of a given "host" region (in this case, the soil). For this constraint, the translational degrees of freedom for the embedded nodes that define the elements of the geocell shell elements are constrained to interpolated values of the corresponding degrees of freedom of the host element (Hibbit et al. 2017). The unreinforced models maintained the same boundary and loading conditions, but had no embedded geocell. To avoid computational issues due to large differential stiffness between the steel plate and the surrounding soil, uplift movements were applied directly to soil beneath the geocell, omitting actual modeling of the anchor plate.

7.2. Material Properties and Meshing

The granular backfill soil was modeled as a non-associative elastic-plastic material, obeying the 3D Drucker-Prager (D-P) yield criterion (Leshchinsky and Ling, 2013). Although more complex constitutive models are available, the D-P model was deemed appropriate as its strength and yield properties are dependent on volumetric strain and stress levels that may play a role in the observed uplift behavio~~u~~r. Furthermore, the D-P constitutive laws have been demonstrated to be effective in the modelling of granular materials in various geosynthetic applications (Yoo and Kim , 2008; Leshchinsky and Ling, 2013, Ambauen et al. 2015). The deformation and strength properties of the backfill soil were calibrated to match data from triaxial compression tests (i.e stress-strain responses under three confining pressures), so as to demonstrate no more than 10%-15% difference between the numerical results and the triaxial test results. The soil properties used in the analysis are summarized in **Table 6**. A Poisson's ratio of 0.3 and a Young's Modulus of 70 MPa were determined from an appropriate capture of the load-displacement response of the reinforced and unreinforced anchoring systems. A comparison to past literature demonstrates that these values were found to be very reasonable for sand (v=0.3 to 0.45, E_s=5 MPa to 180 MPa, Bowles 1983).

A small value of cohesion (1 kPa) was assigned to the backfill soil in order to improve numerical stability and to avoid modeling difficulties, such as localization issues at or near singularities. The geocell was modeled as a purely elastic material since the soil tends to demonstrate large strains and collapse before significant

Formatted: Not Highlight

plasticity occurs in the relatively extensible geocell materials. The geocell pockets were modeled with a hexahedron shape (**Fig. 10a**) as opposed to the actual pseudo-sinusoidal shape used in the experiments as it simplifies meshing and benefits model convergence - an assumption made in prior FE modeling of geocell (Yang, 2010; Leshchinsky and Ling, 2012). The Young's modulus of the geotextile material (HDPE, obtained from Tension test according to ASTM D4632-08) used in the analysis and its Poisson's ratio are considered 800 MPa and 0.33, respectively.

The unreinforced model consisted of approximately 45,000 elements and 50,000 nodes for the unreinforced case and approximately 65,000 elements and 70,000 nodes for the reinforced case (**Fig. 10b**). A majority of these elements were placed near the anchor plate, as its behavior was of most interest and it is the location where deformation was expected to be concentrated. The soil is represented with tetrahedral 8-noded elements with reduced integration (C3D8R), while the geocell was modeled as a shell meshed with 4-noded quadrilateral reduced integration elements (S4R). A sensitivity analysis was performed to ensure that the meshing employed for each type of model was adequate. These results demonstrate that the use of 40,000 and 60,000 elements for unreinforced and reinforced cases, respectively, were appropriate for solution accuracy.

7.3. Comparison between results from ABAQUS analyses and physical tests

Comparison between the near full-scale experiments and numerical modeling load-displacement curves considering embedment ratios of 1.5, 2, 2.5 and 3 with and without geocell reinforcement are shown in **Fig. 11.** Although analyses of the 150 mm plate anchors show agreement of peak loads for the unreinforced case, rather large overestimates of peak load were obtained for the reinforced cases with some post-peak instability observed in the estimated load – perhaps attributable similarity in the plate and geocell pocket size. For these reasons the 150 mm data are not presented here. The selected constitutive model does not capture the post-peak softening well, a common limitation in FE modeling. For smaller plate anchor sizes (225×225 mm), numerical perturbations arise due to the explicit solver maintaining stability under large deformations, particularly with small overburden. However, the maximum observed uplift load and the initial load-displacement response are satisfactorily captured for all cases.

7.4. Soil Displacement under Uplift Loading

The plate size, the embedment ratio, and the presence of geocell affected the uplift mechanism observed in the soil. For example, the presence of geocell results in a larger region that must deform to allow yield (**Fig. 12**). The presence of the confined soil within the geocell mattress results in mobilization of tensile stress in the geocell, passive resistance of the confined soil, and a wider distribution of stress displacements that must occur with uplift. The increased uplift capacity can be attributed to this load-spreading phenomenon. As seen in **Fig. 12**, the displacement contours for the reinforced case begin further from the plate, a distinct difference from the unreinforced case, where a rather narrow column of soil above is displaced directly from the edges of the plate. In **Fig. 13**, this phenomenon is further demonstrated by comparing the locus of maximum plastic shear within the soil. The angle between this inferred shear surface and the vertical (θ) is approximately 19.5° for both unreinforced and reinforced cases. This corroborates observations about uplift failure surfaces oriented $\phi/2$ from the vertical in the literature (Meyerhof and Adams, 1968). However, as opposed to the unreinforced case, which exhibits the onset of shear originating a distance of $B/2$ from the centerline, the presence of geocell results in almost double the distance from the centerline to the point at which plastic strain occurs during uplift (**Fig. 13**).

This reinforcing phenomenon of the geocell is further demonstrated by comparing soil heave, as shown in **Fig. 14**. In this plot, the black lines represent the vertical displacement computed at the surface, corresponding to plate displacement of 20 mm for the unreinforced and reinforced cases; while the red lines represent the vertical displacements measured at the surface for the reinforced cases corresponding to the peak/ultimate uplift loads for the unreinforced cases of similar configuration. This plot shows that when the geocell is present (red lines), the heave is less than 10% of that experienced with the unreinforced installation (black lines) for the same load. However, when comparing heave profiles at the end of the numerical analysis (plate displacement of 20 mm), the geocell-reinforced soil demonstrates a significantly wider region of displacement (approximately 30-50% wider), indicating a larger zone in which the uplift resistance is gained due to the geocell's presence (**Fig. 14**). As expected, increasingly wide plates exhibit wider surface displacements, a behavior that is more pronounced with reinforcement. Furthermore, increasing embedment depth resulted in a decrease in surface heave as the deformation is dispersed within more material before reaching the surface. The heave realized at the surface displayed a relatively circular shape for both reinforced and unreinforced conditions, particularly with increasing embedment depth. The redistribution of stresses due to the geocell exaggerates this behavior.

Table 7 lists the maximum distance from the center of plate at which heave is discernable (although the affected zone is only approximately circular the term 'maximum surface heave radius' is used). Values as measured in the experiments and in the numerical models for different arrangements are given for a plate displacement of 20 mm (the end of analysis). This table indicates good agreement between computed and measured results.

7.5. Geocell Deformations and Strains

As plate uplift occurs, part of the overlying geocell deforms, providing tensile resistance and developing frictional forces along the top and bottom boundaries of the displacing mattress (**Fig. 15**). As vertical uplift increases, the relative mobilization width of geocell confinement (b') increases. With excessive displacement, stiffer geocell material, or more ductile soil, it is possible that the mobilized geocell width would be equivalent to the entire width of the geocell (i.e. b=b'), but that was never the case for the values of the parameters studied here. For the cases investigated, the mobilized geocell width is compared by means of longitudinal strain in geocell mattress (**Fig. 16**). The longitudinal strain remains around 0.4% in the center of geocell for all cases, while reaching a maximum value of approximately 2.5-3.5% at the edge of anchor plate, eventually decreasing to zero at some distance from the edge of the plate. Approximately 50% of the geocell width undergoes enough strain to develop frictional forces between the geocell surfaces and the surrounding soil in the cases studied. As the geocell becomes stiffer, soil more ductile or uplift displacements greater, it is possible that the mobilized geocell width may approach the width of the reinforcements, but one must be careful to prevent excessive displacement during uplift so as to prevent failure.

8. Summary and Conclusions

The presented study demonstrates the results of a series of near full-scale experiments and numerical models performed on plate anchors embedded in sand with and without geocell reinforcement. The parameters studied in the testing program and numerical analyses include geocell reinforcement, and anchor width and embedment depth. Conclusions include:

- The presence of the geocell layer increased the plate anchor capacity significantly, a phenomenon that can be attributed to a wider region of mobilized, vertically-displacing overburden soil. It also resulted in sustained uplift resistance at larger displacements~~, ~~; different from~~than~~ the distinct softening behavior observed for post-peak conditions in unreinforced systems. The wider mobilization of overburden soil is highlighted by an observed pressure reduction of between 28% and 41% when a geocell layer was present. Similarly, the dispersion angle (relative to the vertical) was measured to be about 19.3° and 24.7° for unreinforced and reinforced systems, respectively, indicating the greater load distribution achieved from the presence of a geocell layer.

- Both the peak and residual uplift loads of unreinforced and reinforced systems increase approximately linearly with anchor embedment depth, irrespective of the anchor width. For the larger width anchors (225 and 300 mm), the rate of increase in both the peak and residual uplift loads with embedment depth is significantly greater than for small anchors (150 mm width), whether reinforced or not, seemingly indicating some kind of transition in load ~~dispersion~~ spreading behavior from that experienced with punching shear failure (small anchors) to that associated with general failure (terms as per Vesic, 1963). There is significant difference between the upward displacements corresponding to the maximum uplift load and the residual loads of unreinforced system.
- As expected, the breakout factor increases with embedment depth and decreases with increasing anchor width for both reinforced and unreinforced conditions. It is higher for geocell-reinforced conditions than unreinforced conditions, irrespective of embedment depth and width of anchor.
- Calibrated FE simulations were performed to replicate physical testing, demonstrating reasonable agreement with experimental observations. These numerical models captured the performance of the reinforced soil reasonably well, demonstrating mobilized reinforcement tributary area, lowered uplift stresses, shear occurring in overburden soil, and reduced heaved from the presence of the geocell, but could not sufficiently capture the characteristic post-peak softening behavior observed in the physical unreinforced tests. Future work could include more complex constitutive models that capture this important behavior.
- Corroborating prior work, it is demonstrated that there is a scale effect that should be considered for square plate anchors – specifically, increasing the plate dimensions for fixed embedment ratios will result in lower breakout factors.

The experiments and numeric results were obtained for only one type of soil, one type of geocell characteristics and one size of geocell (i.e. height and pocket). In spite of these limitations, the uplift plate anchor tests and the matching numerical simulations carried out in the present study provide considerable encouragement for the use of geocell reinforcement, in improving the behavior of anchor plate. However, future studies could extend the presented numerical techniques to assess relevant design parameters, such as soil type, plate size, embedment depth, anchor and reinforcement geometric configuration, and stiffness of geosynthetic materials towards establishing more robust design criteria for geocell-reinforced anchoring, accounting for the influence of geocell-infill interaction properties, and the influence of varying geocell specifications (i.e roughness, shape, and presence of perforations). This study, however, highlights the mechanisms that one must consider when extending this concept further. Future work could also parameterize the effects of these material properties on mobilization of geocell tensions.

Acknowledgment

The authors thank DuPont de Nemours, Luxembourg, and their UK agents, TDP Limited, for providing the geocell reinforcement used in this test program.

References

American Society for Testing and Materials, 2007. *Standard Test Method for Density and Unit Weight of Soil in Place by the Sand-Cone Method*. ASTM International, D1556.

American Society for Testing and Materials, 2008. *Standard Test Method for Grab Breaking Load and Elongation of Geotextiles*. ASTM Int’~~ernational~~l., D4632.

American Society for Testing and Materials, 2011. *Standard Practice for Classification of Soils for Engineering Purposes (Unified Soil Classification System).* ASTM ~~International~~Int’l., D 2487-11.

American Society for Testing and Materials, 2012. S*tandard Test Methods for Laboratory Compaction Characteristics of Soil Using Modified Effort*. ASTM Int’l., D 1557-12.

Ambauen, S., Leshchinsky, B., Xie, Y., & Rayamajhi, D. (2015). Service-state behavior of reinforced soil walls supporting spread footings: a parametric study using finite-element analysis. *Geosynth. Int’l*, ~~*Geosynth. Int.,*~~ 23(3), 156-170.

Biabani, M. M., Indraratna, B., Trung Ngo. N., 2016. Modelling of geocell-reinforced subballast subjected to cyclic loading. *Geotext.~~iles and~~ Geomem~~branes~~*, 44 (March), 489–503.

Binquet, J. and Lee, K.L., 1975. Bearing capacity tests on reinforced earth slabs. *J Geotech. Eng’g Div*., ASCE, 101 (GT12), 1241-1255.

Bhattacharya, P., Kumar, J., 2014. Pullout capacity of inclined plate anchors embedded in sand. *Canadian Geotech. J.~~nical Journal~~*, 51(11), 1365-1370.

Bhattacharya, P., Kumar, J., 2015. Uplift Capacity of Strip and Circular Anchors in Soft Clay with an Overlay of Sand Layer. *Geotech.~~nical and~~& Geolog~~ica~~.~~l Engineering~~Eng’g.*, 33(6), 1475-1488.

Bowles, J.E., 1996. *Foundation Analysis and Design*. 5th edn., McGraw-Hill, New York, 1175pp.

Formatted: English (United States)

Formatted: English (United States)

Formatted: Font: Italic

Formatted: Font: Italic

Field Code Changed

Formatted: Font: Italic

Formatted: Font: Italic

Formatted: Font: Italic

Formatted: Font: Italic

Formatted: Font: Italic

Formatted: Font: Italic

Formatted: Font: Italic

Choudhury, D., Subba Rao, K. S., 2005. Seismic uplift capacity of inclined strip anchors. *Canadian Geotech. J.,* ~~*Canadian Geotechnical Journal,*~~ 42(1), 263-271.

Choudhary, A. K., Dash, S. K., 2013. Uplift behaviour of horizontal plate anchors embedded in geocell-reinforced sand, ~~*Proceedings*~~ *Proc.* ~~*of*~~ *Indian* ~~*Geotechnical*~~ *Geotech.* ~~*Conference*~~ *Conf.,* December 22-24, Roorkee.

Consoli, N. C., Thomé, A., Girardello, V., Ruver, C. A., 2012a. Uplift behavior of plates embedded in fiber-reinforced cement stabilized backfill. *Geotext. & Geomem.,* 35 (December), 107–111

Consoli, N. C., Ruver, C.A., Girardello, V., Festugato, L., Thomé, A., 2012b. Effect of polypropylene fibers on the uplift behavior of model footings embedded in sand. *Geosynth. Int'l* ~~*Geosynthetics International*~~,s 19(1), 79-84

Das, B., Seeley, G. 1975. Breakout resistance of shallow horizontal anchors, *J*~~*ournal of the*~~ *Geotech*~~*nica.l*~~ ~~*Engineering*~~*Eng'g.*, ASCE, 101(9), 999-1003

Dash S.K., Sireesh, S., Sitharam, T.G., 2003. Model studies on circular footing supported on geocell reinforced sand underlain by soft clay. *Geotext. & Geomem.,* ~~Geotextiles and Geomembranes,~~ 21 (4), 197–219

Dawson, A.R., Lee, R.G., 1988, Full scale foundation trials on grid-reinforced clay, *Geosynthetics for Soil Improvement*, Ed. Holtz R, ASCE ~~Geotechnical~~ Geotech. Special ~~Publication~~Pub'n, 18, 27-147.

Deskmukh, V.B., Dewaikar, D.M., Deepankar Choudhury., 2010. Computations of uplift capacity of pile anchors in cohesionless soil. *Acta Geotechnica*, 5 (2), 87 – 94.

Dickin, E., 1988. Uplift behavior of horizontal anchor plates in sand, *J Geotech. Eng'g,* ~~Journal of geotechnical engineering~~, ASCE. 114(11), 1300-17.

Dickin, E., Laman, M., 2007. Uplift response of strip anchors in cohesionless soil', Advances in ~~Engineering~~ Eng'g Software, 38 (8–9), 618–25.

Dickin, E.A., Leung, C.F., 1990. Performance of piles with enlarged bases subjected to uplift forces. *Canadian Geotech. J.,* ~~Canadian Geotechnical Journal.,~~ 27(5), 546–556.

Frydman, S., Shaham, I., 1989. Pullout capacity of slab anchors in sand, *Canadian Geotech. J.,* ~~Canadian Geotechnical Journal,~~ 26(3), 385–400.

Field Code Changed
Formatted: Font: Italic
Formatted: Font: Italic
Formatted: Font: Italic
Formatted: Font: Italic
Formatted: Font: Italic
Formatted: Font: Italic
Formatted: Font: Italic
Field Code Changed
Field Code Changed
Field Code Changed
Field Code Changed
Field Code Changed
Formatted: Font: Italic
Formatted: Font: Italic
Formatted: Font: Italic
Formatted: Font: Italic

Ganesh, R., Sahoo, J. P., 2016. Uplift capacity of horizontal strip plate anchors adjacent to slopes considering seismic loadings. Soils ~~and~~ & Foundations, 56(6), 998-1007.

Ghaly, A., Hanna, A., 1994. Model investigation of the performance of single anchors and groups of anchors, *Canadian Geotech. J.*, ~~**Canadian Geotechnical Journal.**~~ 31(2), 273-284

Ghosh, A., Bera, A. K., 2010. Effect of Geotextile Ties on Uplift Capacity of Anchors Embedded in Sand, *Geotech. & Geolog. Eng'g.*~~Geotechnical and Geological Engineering~~, 28(5), 567–77.

Goel, S., Shalini., Patra, N.R., 2006. Break out resistance of inclined anchors in sand, *Geotech. & Geolog. Eng'g.*, ~~Geotech Geol Eng.~~ 24 (6), 1511-1525.

Guo, J., Han, J., Schrock, S.D., Parsons, R.L., 2015. Field evaluation of vegetation growth in geocell-reinforced unpaved Shoulders, *Geotext. & Geomem.*, ~~Geotextiles and Geomembranes,~~ 43(5), 403–411.

Hibbett, Karlsson, & Sorensen (2017). *ABAQUS/explicit: User's manual* (Vol. 1). Hibbett, Karlsson & Sorensen.

Hegde, A., Sitharam, T. G., 2015. 3-Dimensional numerical modelling of geocell reinforced sand beds, *Geotext. & Geomem.*, ~~Geotextiles and Geomembranes,~~ 43(2), 171–81.

Honda, T., Hirai, Y., Sato, E., 2011. Uplift capacity of belled and multi-belled piles in dense sand. *Soils ~~and~~ & Foundations*, 51 (3), 483-496.

Horpibulsuk, S., Niramitkorburee, A., 2010. Pullout resistance of bearing reinforcement embedded in sand. *Soils ~~and~~ & Foundations*, 50 (2), 215-228.

Ilamparuthi, K., Dickin, E. A., 2001. The influence of soil reinforcement on the uplift behaviour of belled piles embedded in sand, *Geotext. & Geomem.*, ~~Geotextiles and Geomembranes,~~ 19(1), 1–22.

Ilamparuthi, K., Dickin, E. A., Muthukrisnaiah, K., 2002. Experimental investigation of the uplift behaviour of circular plate anchors embedded in sand, *Canadian Geotech. J.*, ~~Canadian Geotechnical Journal,~~ 39 (3) 648–664.

Indraratna, B., Biabani, M.M., Nimbalkar, S., 2015. Behavior of Geocell-Reinforced Subballast Subjected to Cyclic Loading in Plane-Strain Condition. ~~*Journal of Geotechnical and Geoenvironmental Engineering*~~*J. Geotech. & Geoenviron. Eng'g.*, ASCE. 141(1), 16pp.

Formatted: Font: Bold

Formatted: Font: Italic

Field Code Changed

Formatted: Font: Italic

Field Code Changed

Field Code Changed

Formatted: English (United States)

Formatted: English (United States)

Formatted: English (United States)

Formatted: English (United States)

Field Code Changed

Formatted: English (United States)

Formatted: English (United States)

Field Code Changed

Formatted: English (United States)

Formatted: English (United States)

Formatted: English (United States)

Field Code Changed

Formatted: Font: Italic

Formatted: Font: Italic

Jones, R.H., Lee, R.G. and Dawson A.R., 1991. Full-scale trials of grid reinforced soil foundations on alluvium, *Quarternary Engineering Geology*, Eng. Geol. Sp. Publn. No. 7, eds. Forster, A, Culshaw M G, Cripps S C, Little J A and Moon C F, Geol. Soc., London, pp.643-649.

Karpurapu, R., Bathurst, R. J., 1995. Behaviour of geosynthetic reinforced soil retaining walls using the finite element method. *Computers & Geotech.,* ~~Computers and Geotechnics.~~ 17(3), 279-299

Keskin, M. S., 2015. Model studies of uplift capacity behavior of square plate anchors in geogrid-reinforced sand. ~~Geomechanics~~ Geomech. ~~and~~ & ~~Engineering~~Eng'g., 8(4), 595-613.

Khan, A. J., Mostofa, G., Jadid, R., 2017. Pullout resistance of concrete anchor block embedded in cohesionless soil. Geomech. & Eng'g., ~~Geomechanics and Engineering,~~ 12(4), 675-688.

Khatri, V.N., Kumar, J., 2009. Vertical uplift resistance of circular plate anchors in clays under undrained condition. *Computers & Geotech.,* ~~Computers and Geotechnics,~~ 36 (8), 1352–1359.Koerner, R. M. (2012). Designing with geosynthetics (Vol. 1). Xlibris Corporation.

Kouzer, K., Kumar, J., 2009. Vertical uplift capacity of two interfering horizontal anchors in sand using an upper bound limit analysis, *Computers* ~~*and*~~ *&* ~~*Geotechnics*~~*Geotech.*, 36 (6), 1084–1089.

Krishnaswamy, N. R., Parashar, S. P., 1994. Uplift behaviour of plate anchors with geosynthetics, *Geotext. & Geomem.,* ~~Geotextiles and Geomembranes,~~ 13(2), 67–89.

Kumar, J., Bhoi, M. K., 2009. Vertical uplift capacity of equally spaced multiple strip anchors in sand, *Geotech. & Geolog. Eng'g.,* ~~Geotechnical and Geological Engineering,~~ 27(3), 461–72.

Kumar, B. R. P., & Rao, N. R. (2000). Increasing pull-out capacity of granular pile anchors in expansive soils using base geosynthetics. *Canadian Geotech. J.,* ~~*Canadian Geotechnical Journal,*~~ *37*(4), 870-881.

Kumar, B. R. P., 2016. Influence of Geogrid Reinforcement on Pullout Response of Granular Pile-Anchors (GPAs) in Expansive Soils. *Indian Geotech*~~*nical*~~*. J.*~~ournal~~, 46 (4), 437–~~–~~444.

Lee, K. F., Davidson, J. F., Akroyd, J., Kraft, M., 2014. Lifting a buried object: Reverse hopper theory, *~~Chemical~~ Chem. ~~Engineering~~ Eng'g ~~Science~~Sci.*, 105, 198–207.

Leshchinsky, B., Ling, H., 2012. Effects of geocell confinement on strength and deformation behavior of gravel. *J. Geotech. & Geoenviron. Eng'g.,* ASCE. ~~Journal of Geotechnical and Geoenvironmental Engineering, ASCE,~~ 139(2), 340-352.

Field Code Changed

Formatted: Font: Italic

Formatted: Not Highlight

Formatted: Font: Italic, Not Highlight

Formatted: Not Highlight

Formatted: Font: Italic

Field Code Changed

Leshchinsky, B., Ling, H. I., 2013. Numerical modeling of behavior of railway ballasted structure with geocell confinement, *Geotext. & Geomem.*, ~~Geotextiles and Geomembranes,~~ 36, 33–43.

Liu, J., Liu, M., Zhu, Z., 2012. Sand Deformation around an Uplift Plate Anchor. *J. Geotech. & Geoenviron. Eng'g.*, ASCE. ~~Journal of Geotechnical and Geoenvironmental Engineering,~~ 138(6), 728-737.

Merifield, R. S., Sloan, S. W., 2006. The ultimate pullout capacity of anchors in frictional soils, *Canadian Geotech. J.*, ~~Canadian Geotechnical Journal,~~ 43(8), 852–68.

Meyerhof, G. G., Adams, J. I., 1968. The Ultimate Uplift Capacity of Foundations, *Canadian Geotech. J.*, ~~Canadian Geotechnical Journal,~~ 5(4), 225–44.

Moayedi, H., Mosallanezhad, M., 2017. Uplift Resistance of Belled and Multi-Belled Piles in Loose Sand. *Measurement*, 109(October), 346-353

Moghaddas Tafreshi, S.N., Rahimi M., 2012. A simplified pseudo-dynamic method of reinforced retaining wall subjected to seismic loads. *Materialy 15 WCEE*, Lisboa.

Moghaddas Tafreshi, S.N., Dawson, A.R., 2012. A comparison of static and cyclic loading responses of foundations on geocell-reinforced sand. *Geotext. & Geomem.*, ~~Geotextiles and Geomembranes~~ 32(June), 55-68.

Moghaddas Tafreshi, S.N., Khalaj, O., Dawson, A.R., 2013. Pilot-scale load tests of a combined multi-layered geocell and rubber-reinforced foundation. *Geosynth. Int'l*, ~~Geosynth. Int.~~ 20 (3), 143-161.

Moghaddas Tafreshi, S. N., Javadi, S., Dawson, A.R., 2014. Influence of geocell reinforcement on uplift response of belled piles, *Acta Geotechnica*, 9(3), 513–28.

Moghaddas Tafreshi, S.N., Sharifi, P., Dawson, A.R., 2016. Performance of circular footings on sand by use of multiple-geocell or-planar geotextile reinforcing layers. *Soils & Foundations*, ~~Soils and Foundations~~ 56 (6), 984-997.

Murray, E., Geddes, J., 1987. Uplift of anchor plates in sand. *J. Geotech. Eng'g.*, ASCE, ~~Journal of geotechnical engineering, ASCE,~~ 113(3), 202-215.

Oliaei, M., Kouzegaran, S., 2017. Efficiency of cellular geosynthetics for foundation reinforcement. *Geotext. & Geomem.*, ~~Geotextiles and Geomembranes,~~ 45(2), 11-22.

Ouria, A., Mahmoudi, A., 2018. Laboratory and numerical modeling of strip footing on geotextile-reinforced sand with cement-treated interface. *Geotext. & Geomem.,* ~~Geotextiles and Geomembranes,~~ 46(1), 29-39

O'Shaughnessy, V., Garga, V.K., 2000, Tire-reinforced earthfill. Part 2: Pull-out behaviour and reinforced slope design, *Canadian Geotech. J.,* ~~Canadian Geotechnical Journal,~~ 37(1), 97-116.

Phani Kumar, B.R., Sharma, R.S., Srirama Rao, A., Madhav, M.R., 2004, Granular Pile – Anchor Foundation (GPAF) System for Improving the Engineering Behaviour of Expansive Clay Beds. *Geotech.Testing J.*, ASTM, 27, (3), 279-287.

Rangari, S. M., Choudhury, D., Dewaikar, D. M., 2013. Computations of Seismic Passive Resistance and Uplift Capacity of Horizontal Strip Anchors in Sand, *Geotech. & Geolog. Eng'g.,* ~~Geotechnical and Geological Engineering,~~ 31(2), 569–80.

Rao, A. S., Phani Kumar, B. R., Increasing pull-out capacity of granular pile anchors in expansive soils using base geosynthetics, *Canadian Geotech. J.*, 37, 870-881

Ravichandran, P. T., Ilamparuthi, K., Touffeq, M. M., 2008. Investigations on Uplift Behaviour of Plate Anchor in Reinforced Sand Bed. *Electronic ~~Journal of~~J ~~Geotechnical~~ Geotech. ~~Engineering~~Eng'g.*, 13, 1-8.

Rowe, R. K., Davis, E. H., 1982. The behaviour of anchor plates in sand, *Geotechnique*, 32(1), 25–41.

Sabatini, P. J., Pass, D. G., Bachus, R. C., 1999. *Geotechnical engineering circular no. 4: ground anchors and anchored systems* (No. FHWA-IF-99-015).

Sakai, T., Tanaka, T., 2007. Experimental and Numerical Study of Uplift Behavior of Shallow Circular Anchor in Two-Layered Sand, *J. Geotech. & Geoenviron. Eng'g.,* ASCE. ~~Journal of Geotechnical and Geoenvironmental Engineering,~~ 133(4), 469–477.

Sahoo, J. P., Khuntia, S., 2017. Lower bound solutions for uplift capacity of strip anchors adjacent to sloping ground in clay. *Marine Georesources ~~and~~ & Geotechnology* (In Press)

Shin, J., Kim, J., Chang, H. J. 2016. Anchor plate effect on the breakout capacity in tension for thin-walled concrete panels. *Eng'~~ineering~~ Structures*, 106, (1) 147-153.

Song, Z., Hu, Y., Randolph, M.F., 2008. Numerical simulation of vertical pullout of plate anchors in clay. *J. Geotech. & Geoenviron. Eng'g.,* ASCE. ~~J Geotech. Geoenviron. Eng., ASCE,~~ 134 (6), 866~~–~~–887.

Field Code Changed

Formatted: Font: Italic

Field Code Changed

Formatted: Font: Italic

Formatted: Font: Italic

Formatted: Font: Italic

Field Code Changed

Song, Z., Hu, Y., O'Loughlin, C., Randolph, M.F., 2009. Loss in Anchor Embedment during Plate Anchor Keying in Clay. *J. Geotech. & Geoenviron. Eng'g.*, ASCE. ~~Journal of Geotechnical and Geoenvironmental Engineering.~~ 135(10), 1475–1485.

Song, F., Liu, H., Chai, H., Chen, J., 2017. Stability analysis of geocell-reinforced retaining walls. *Geosynth. Int'l*, ~~Geosynthetics International.~~ 24(5), 442–450.

Tagaya, K., Scott, R. F., Aboshi, H., 1988. Pullout resistance of buried anchor in sand. *Soils ~~and~~ & Foundations*, 28(3), 114–30.

Tavakoli Mehrjardi, G. h., Moghaddas Tafreshi, S. N., Dawson, A. R., 2012. Combined use of geocell reinforcement and rubber–soil mixtures to improve performance of buried pipes. *Geotext. & Geomem.*, ~~Geotextiles and Geomembranes,~~ 34 (October), 116–130.

Tanyu, B.F., Aydilek, A.H., Lau, A.W., Edil, T.B., Benson, C.H., 2013. Laboratory evaluation of geocell-reinforced gravel subbase over poor subgrades. *Geosynth. Int'l*, ~~Geosynth. Int.~~ 20 (2), 47-61.

Thakur, J. K., Han, J., Pokharel, S. K. Parsons, R. L., 2012. Performance of geocell-reinforced recycled asphalt pavement (RAP) bases over weak subgrade under cyclic plate loading. *Geotext. & Geomem.*, ~~Geotextiles and Geomembranes,~~ 35(December), 14–24.

Tian, Y, Gaudin, C., Cassidy, M.J., 2014. Improving Plate Anchor Design with a Keying Flap. *Geotech. & Geolog. Eng'g.*, ~~Journal of Geotechnical and Geoenvironmental Engineering,~~ 140(5), 13pp.

Tran, V. D. H., Meguid, M. a., Chouinard, L. E. (2013). A finite-discrete element framework for the 3D modeling of geogrid-soil interaction under pullout loading conditions, *Geotext. & Geomem.*, ~~Geotextiles and Geomembranes,~~ 37: 1–9.

Treff, A., 2011. Private Communication with Albert Treff of DuPont de Nemours, Luxembourg.

Trung Ngo. N., Indraratna, B., Rujikiatkamjorn, C., Biabani, M. M., 2016. Experimental and Discrete Element Modeling of Geocell-Stabilized Subballast Subjected to Cyclic Loading. *J. Geotech. & Geoenviron. Eng'g.*, ASCE. ~~Journal of Geotechnical and Geoenvironmental Engineering.~~ 142(4), 14pp

Vahedifard, F., Shahrokhabadi,S., Leshchinsky, D., 2016. Geosynthetic-reinforced soil structures with concave facing profile. *Geotext. & Geomem.*, ~~*Geotextiles and Geomembranes,*~~ 44 (3), 358-365.

Vesic, A. S., 1963. Bearing capacity of deep foundations in sand, *Highway Research Record*, No. 39, 112–153.

Vesic, A. S., 1971. Breakout resistance of objects embedded in ocean bottom, ~~*Journal of the*~~*J. Soil Mech*~~*anics*~~ ~~*and*~~*. & Foundations Div*~~*ision*~~*.*, ASCE, 97(9): 1183–205.

Vishwas, N. K., Kumar, J., 2011. Effect of anchor width on pullout capacity of strip anchors in sand

Canadian Geotech. J., ~~Canadian Geotechnical Journal,~~ 48(3), 511-517.

Wang, D., O'Loughlin, C.D., 2014. Numerical study of pull-out capacities of dynamically embedded plateanchors. *Canadian Geotech. J.,* ~~Canadian Geotechnical Journal,~~ 51(11), 1263-1272.

Yetimoglu, T., Wu, J.T., Saglamer, A., 1994, Bearing capacity of rectangular footings on geogrid-reinforced sand. *J. Geotech. Eng'g.*, ASCE, 120(12), 2083-2099.

Yang, X., 2010. *Numerical Analyses of Geocell-Reinforced Granular Soils under Static and Repeated Loads*. PhD Thes~~s~~is. University of Kansas, USA.

Yoo, C., & Kim, S. B. (2008). Performance of a two-tier geosynthetic reinforced segmental retaining wall under a surcharge load: Full-scale load test and 3D finite element analysis. *Geotextiles and Geomembranes*, 26(6), 460-472.Yoon, Y.W., Heo, S.B., Kim, S.K., 2008. Geotechnical performance of waste tires for soil reinforcement from chamber tests. *Geotext. & Geomem.,* ~~Geotextiles and Geomembranes~~ 26 (1), 100-107.

Zhang, L., Zhao, M., Shi, C., Zhao, H., 2010. Bearing capacity of geocell reinforcement in embankment engineering, *Geotext. & Geomem.,* ~~Geotextiles and Geomembranes,~~ 28(5), 475–82.

Formatted: Font: Italic

Field Code Changed

Field Code Changed

Formatted: Font: Italic

Nomenclature	
A	anchor area
B	width of anchor plate
b	width of geocell mattress

$B_{un.}$, $B_{re.}$	dimension of back-calculated reinforced and unreinforced tributary area 100 mm above the anchor
D	embedment depth of anchor plate
d	geocell pocket size
E_{gc}	geocell Young's modulus
E_s	soil Young's modulus
G_s	specific gravity
h	height of geocell
IF_{peak}	improvement in peak uplift load
IF_{res}	improvement in residual uplift load
$L.SPC$	left soil pressure cell
N_q	*breakout factor*
P_L	ratio of pressure measured in the reinforced case to that in the unreinforced case for the left soil pressure cell
P_{peak}	peak uplift load
P_R	ratio of pressure measured in the reinforced case to that in the unreinforced case for the right soil pressure cell
P_{res}	residual uplift load
$R.SPC$	right soil pressure cell
u_{peak}	peak upward displacement
W	soil weight above the anchor
$\alpha_{un.}$, $\alpha_{re.}$	average value of pressure distribution dispersion angle through unreinforced and reinforced soil
γ	soil unit weight
v	Poisson's ratio
σ_{max}	maximum uplift pressure on top surface of anchor embedded in unreinforced soil
$\sigma_{un.}$, $\sigma_{re.}$	average pressure within soil for unreinforced and reinforced soil 100 mm above anchor
ϕ	soil angle of internal friction
ψ	Angle of dilation

List of Tables

List of Figures

Formatted: Not Highlight

Formatted: Not Highlight

Fig. 3	Test installation prior to loading (a) actual physical model and (b) Schematic representation (units in mm).
Fig. 4	Variation of uplift load with upward displacement of anchor in unreinforced and reinforced systems for different embedment depth and anchor width of (a) B=150 mm, (b) B=225 mm, (c) B=300 mm.
Fig. 5	General relationship between uplift load and displacement with different phases for (a) unreinforced system (b) reinforced systems.
Fig. 6	Variation of peak and residual uplift loads of unreinforced and reinforced bed with embedment depth (D/B) of anchor for different anchor width, (a) peak uplift load (b) residual uplift loads.
Fig. 7	Variation of IF_{peak}, $IF_{res.}$ and $P_{res.}/P_{peak}$ of unreinforced and reinforced bed with embedment depth (D/B) of anchor for different anchor width (a) IF_{peak} and $IF_{res.}$ (b) $P_{res.}/P_{peak}$.
Fig. 8	Variation of breakout factor, N_q of unreinforced and reinforced beds with embedment depth (D/B) of anchor for different anchor width.
Fig. 9	Variation of soil pressure with upward displacement of anchor with width of 300 mm in unreinforced and reinforced bed (a) D/B=2.5 (b) D/B=3.
Fig. 10	(a) Model geometry and boundary conditions and (b) sample mesh of soil and geocell layer.
Fig. 11	Comparison between experiments and numerical modeling load-displacement curves for B=300 mm (a) unreinforced case, (b) reinforced case and for B=225 mm (c) unreinforced case and (d) reinforced case.
Fig. 12	Example displacement contours for B=300 mm and D/B=3, at the end of analysis (plate displacement of 20 mm) (a) unreinforced and (b) reinforced conditions.
Fig. 13	Recorded zones of concentrated plastic shear strain, at the end of analysis (plate displacement of 20 mm) for unreinforced and reinforced systems (a) B=300 mm, (b) B=225 mm, (c) B=150 mm.
Fig. 14	Surface heave for different configuration of anchor model (a) B=300 mm, (b) B=225 mm, (c) B=150 mm (the black lines represent the surface heave at the end of analysis (plate displacement of 20 mm) of the unreinforced and reinforced cases and the red lines represent surface heave for a reinforced case with a load corresponding to the ultimate, unreinforced, uplift capacity).
Fig. 15	(a) Idealized geocell deformations and (b) observed deformations from FE modeling.
Fig. 16	(a) Contours and (b) plot of tensile strain on the top surface of the geocell.

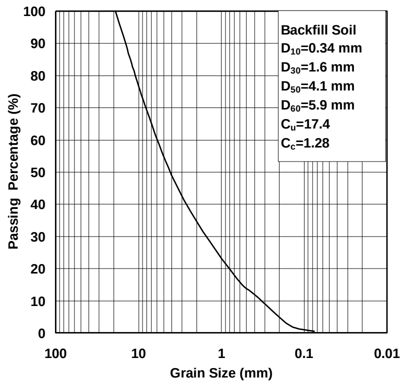

Fig. 1. Grain size distribution curve for backfill soil (as per ASTM D 2487-11).

Formatted: Not Highlight

Formatted: Not Highlight

Fig. 2. A view of geocell (TDP Limited) spread over anchor plate in the test pit.

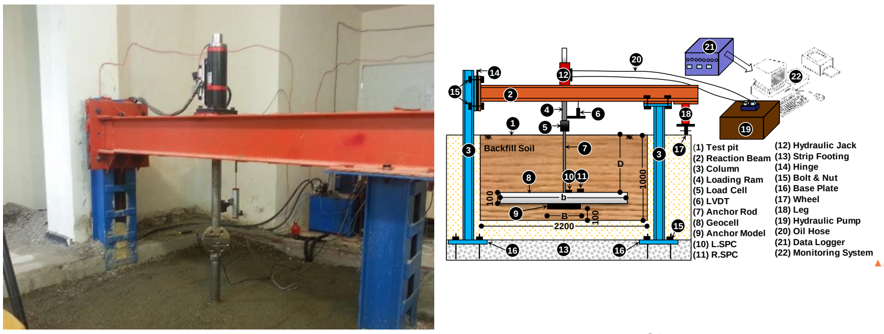

(a) (b)

Fig. 3. Test installation prior to loading (a) actual physical model and (b) Schematic representation (units in mm).

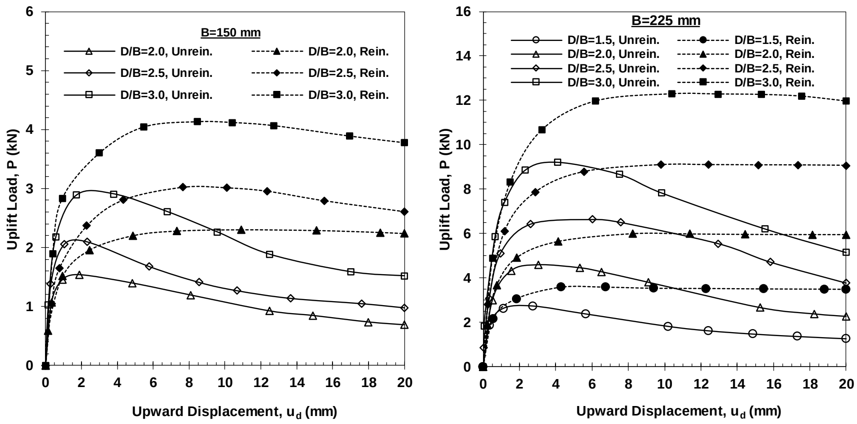

(a) (b)

Formatted: Check spelling and grammar

Formatted: English (United States), Not Highlight

Formatted: Check spelling and grammar

Formatted: English (United States)

Formatted: Check spelling and grammar

Formatted: Not Highlight

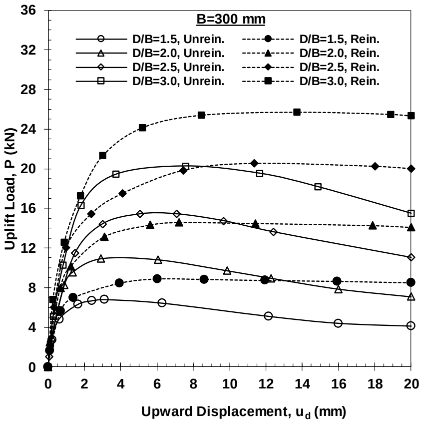

(c)

Fig. 4. Variation of uplift load with upward displacement of anchor in unreinforced and reinforced systems for different embedment depth and anchor width of (a) B=150 mm, (b) B=225 mm, (c) B=300 mm.

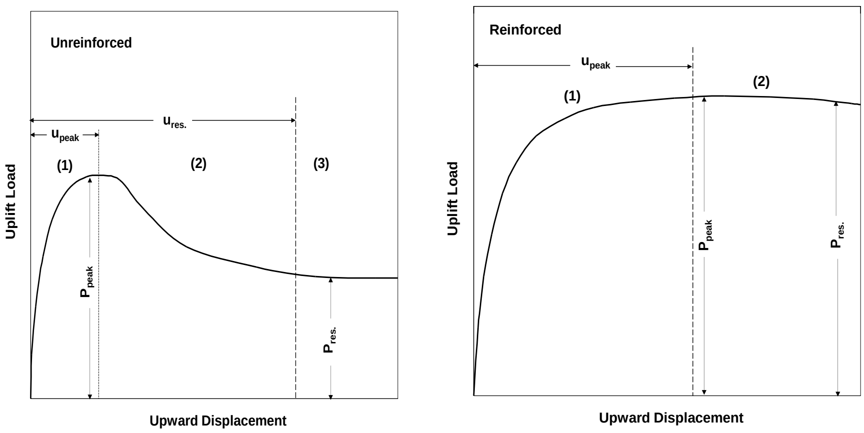

(a) (b)

Fig. 5. General relationship between uplift load and displacement with different phases for (a) unreinforced system (b) reinforced systems.

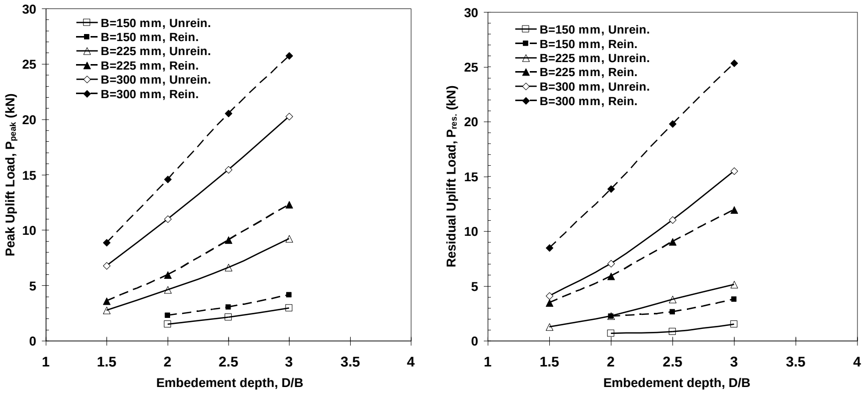

(a) (b)

Fig. 6. Variation of peak and residual uplift loads of unreinforced and reinforced bed with embedment depth (D/B) of anchor for different anchor width, (a) peak uplift load (b) residual uplift loads.

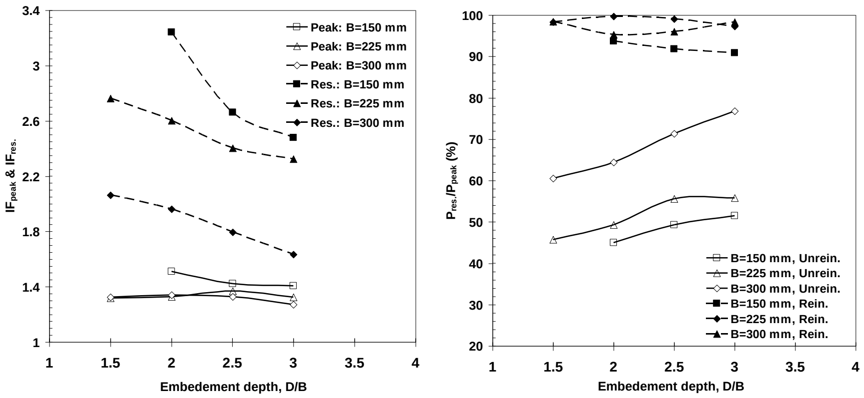

(a) (b)

Fig. 7. Variation of IF_{peak}, $IF_{res.}$ and $P_{res.}/P_{peak}$ of unreinforced and reinforced bed with embedment depth (D/B) of anchor for different anchor width (a) IF_{peak} and $IF_{res.}$ (b) $P_{res.}/P_{peak}$.

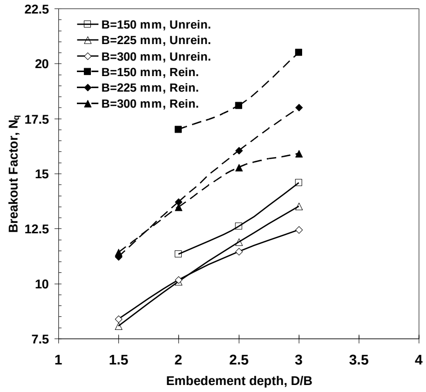

Fig. 8. Variation of breakout factor, N_q of unreinforced and reinforced beds with embedment depth (D/B) of anchor for different anchor width.

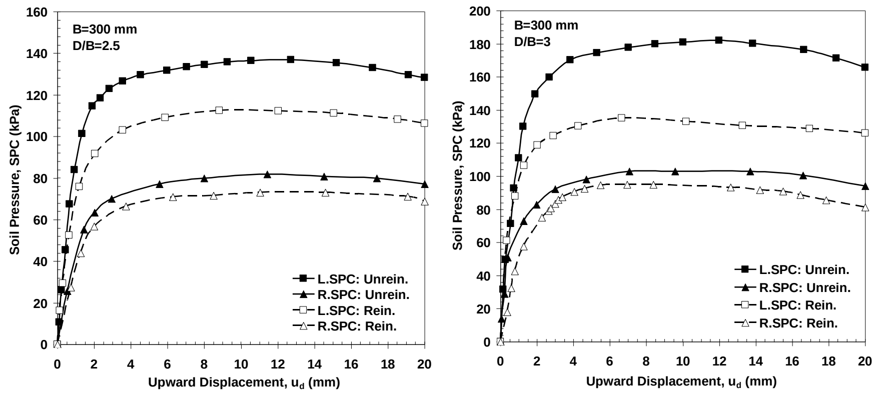

(a) (b)

Fig. 9. Variation of soil pressure with upward displacement of anchor with width of 300 mm in unreinforced and reinforced bed (a) D/B=2.5 (b) D/B=3.

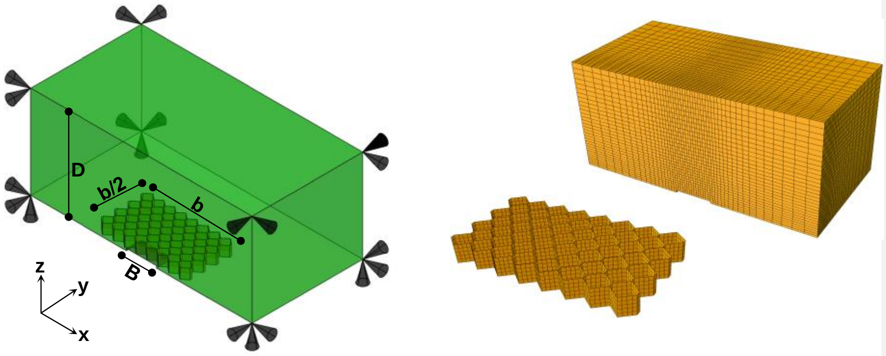

(a) (b)

Fig. 10. (a) Model geometry and boundary conditions and (b) sample mesh of soil and geocell layer.

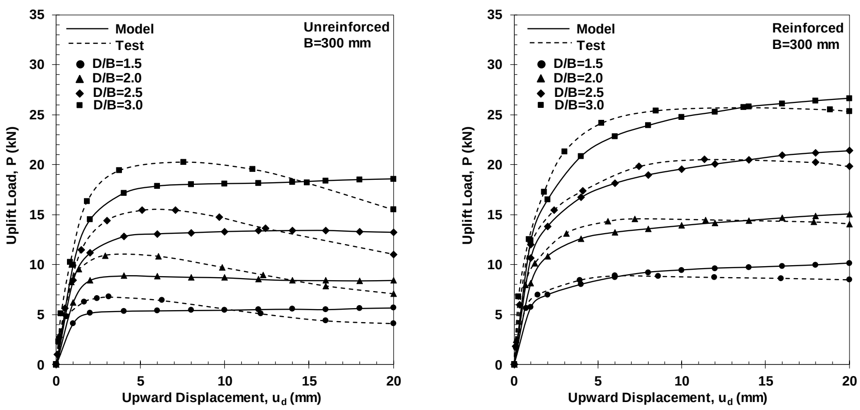

(a) (b)

Formatted: Check spelling and grammar

Formatted: Not Highlight

Formatted: Check spelling and grammar

Formatted: Not Highlight

Formatted: Check spelling and grammar

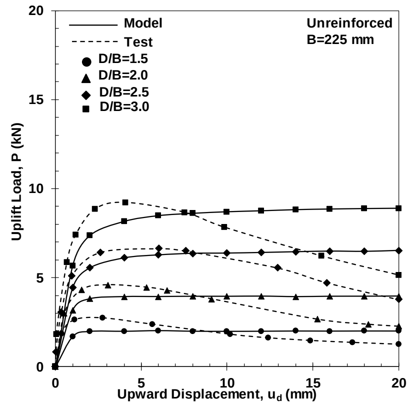

(c)

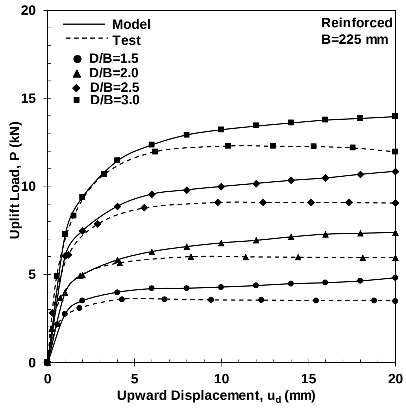

(d)

Fig. 11. Comparison between experimental and numerical modeling load-displacement curves (a) unreinforced (for B=300 mm), (b) reinforced (B=300 mm), (c) unreinforced (B=225 mm) and (d) reinforced (B=225 mm)

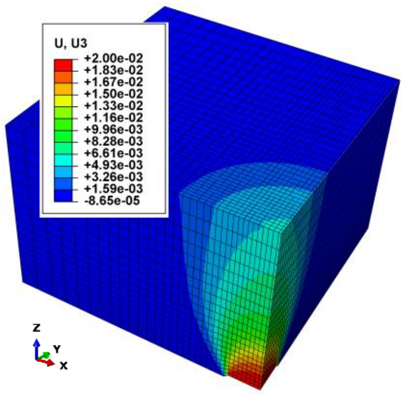

(a)

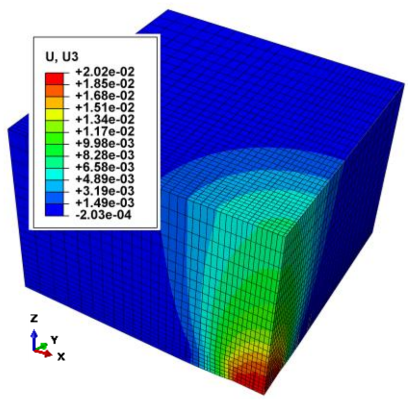

(b)

Fig. 12. Example displacement contours for B=300 mm and D/B=3, at the end of analysis (plate displacement of 20 mm) (a) unreinforced and (b) reinforced conditions.

Formatted: Not Highlight

Formatted: Check spelling and grammar

Formatted: Not Highlight

Formatted: Check spelling and grammar

Formatted: Not Highlight

Formatted: Not Highlight

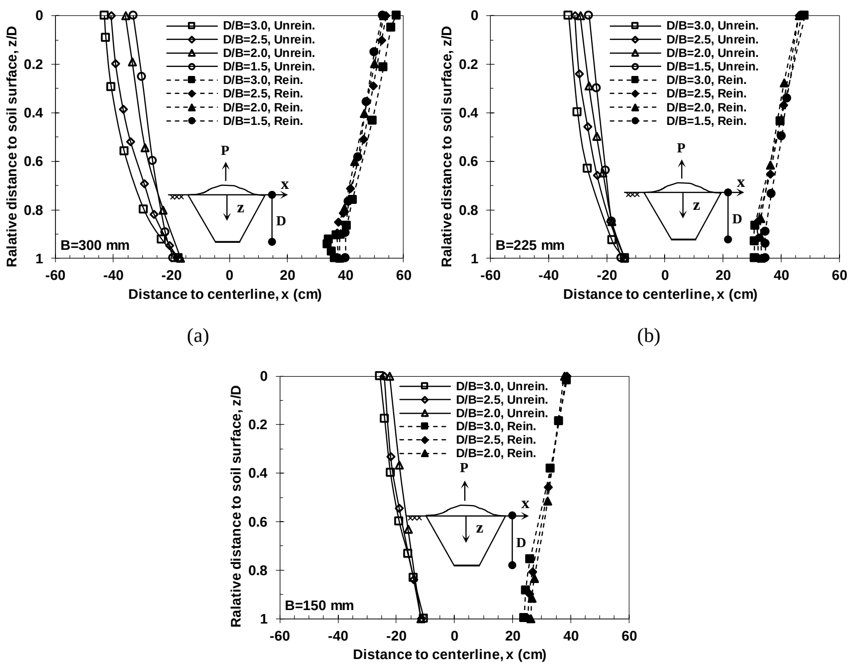

(a) (b)

(c)

Fig. 13. Recorded zones of concentrated plastic shear strain, at the end of analysis (plate displacement of 20 mm) for unreinforced and reinforced systems (a) B=300 mm, (b) B=225 mm, (c) B=150 mm.

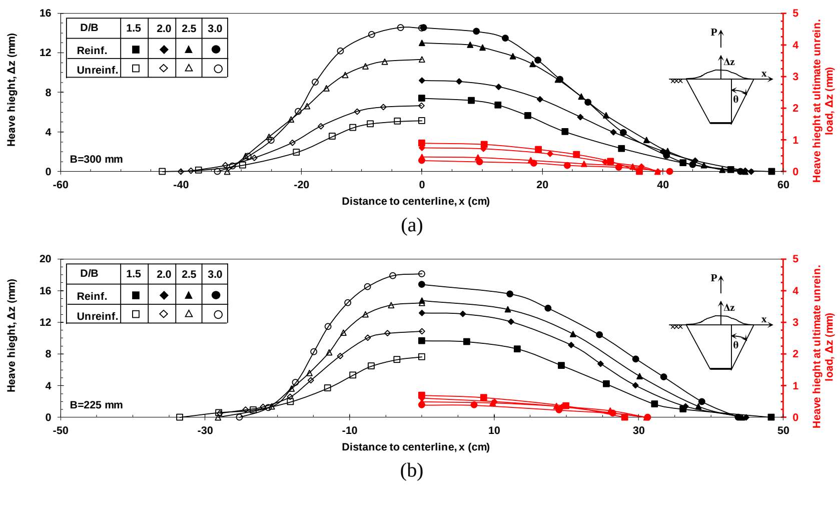

(a)

(b)

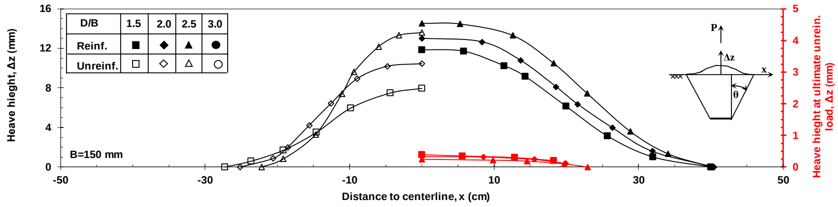

(c)

Fig. 14. Surface heave for different configuration of anchor model (a) B=300 mm, (b) B=225 mm, (c) B=150 mm (the black lines represent the surface heave at the end of analysis (plate displacement of 20 mm) of the unreinforced and reinforced cases and the red lines represent surface heave for a reinforced case with a load corresponding to the ultimate, unreinforced, uplift capacity).

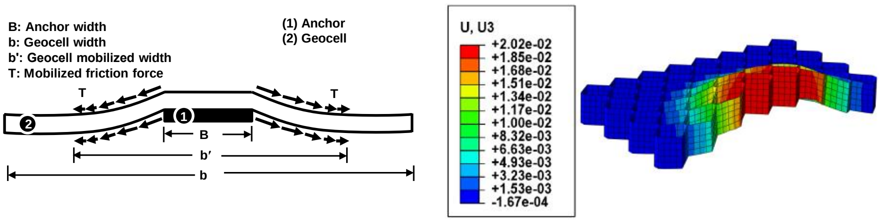

(a) (b)

Fig. 15. (a) Idealized geocell deformations and (b) observed deformations from FE modeling.

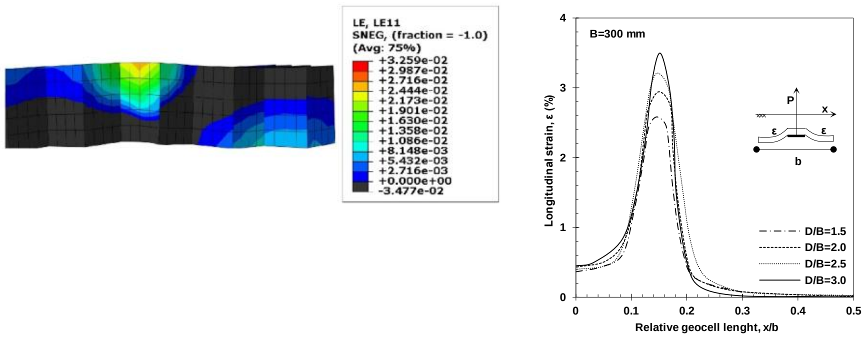

(a) (b)

Fig. 16. (a) Contours and (b) plot of tensile strain on the top surface of the geocell.

Table 1. The engineering properties of the geotextile used in the tests

Description	Value

Type of geotextile	Non-woven
Material	Polypropylene
Area weight (gr/m^2)	190
Thickness under 2 kN/m^2 (mm)	0.57
Thickness under 200 kN/m^2 (mm)	0.47
Tensile strength (kN/m)	13.1
Strength at 5% (kN/m)	5.7
Effective opening size (mm)	0.08

Table 2. Densities of soil for unreinforced and geocell-reinforced layers after compaction (ASTM D 1557-12).

Type of layer	**Average dry density (kN/m^3)**
Unreinforced soil layer	≈18.76*
Geocell-reinforced layer	Between 18.2 and 18.4

*approximately 92% of maximum dry density – see Sec. 3.1

Table 3. Scheme of the uplift tests on anchor in unreinforced and geocell-reinforced backfills (h=100 mm, b/B=3)

test series	**type of test**	**anchor width, B (mm)**	**embedment depth ratio, D/B**	**No. of Tests**	**purpose of the tests**
1	unreinforced	150	2, 2.5, 3	3+4*	Provide baseline estimates regarding uplift capacity
		225, 300	1.5, 2, 2.5, 3	8+10*	
2	geocell-reinforced	150	2, 2.5, 3	3+4*	Highlight the effect of the geocell reinforcement on uplift capacity
		225, 300	1.5, 2, 2.5, 3	8+10*	

**The tests which were performed two or three times to verify the repeatability of the test data. For example, in test Series 2 on anchor plate with width of 150 mm. 7 tests were performed: 3 independent tests plus 4 replicates.*

Formatted: Not Highlight

Formatted: Not Highlight

Table 4. Comparison of upward displacement corresponding to maximum uplift load in reinforced and unreinforced system (displacement in mm)

	B=150 mm			**B=225 mm**			**B=300 mm**		
D/B	$(u_{peak})_{unrein.}$	$(u_{peak})_{rein.}$	Iu_{peak}	$(u_{peak})_{unrein.}$	$(u_{peak})_{rein.}$	Iu_{peak}	$(u_{peak})_{unrein.}$	$(u_{peak})_{rein.}$	Iu_{peak}
1.5	--	--	--	1.54	4.3	2.79	3.11	6.03	1.94

2	1.28	5.82	4.54	2.32	6.05	2.32	4.15	7.22	1.74
2.5	1.55	6.25	4.03	3.42	7.42	2.17	5.59	8.75	1.56
3	2.84	7.24	2.54	4.1	8.1	1.98	7.57	10.85	1.43

Table 5. Comparison of measured soil pressure in unreinforced and geocell-reinforced systems corresponding to peak uplift load of unreinforced system

		Soil pressure corresponding to maximum uplift load of unreinforced system						
B (mm)	D/B	Unreinforced			Reinforced		Ratio of soil pressure in reinforced system to unreinforced system (P)	
		Maximum uplift pressure, σ_{max} (kPa)	L.SPC (kPa)	R.SPC (kPa)	L.SPC (kPa)	R.SPC (kPa)	$P_{L.}$	P_R
300	1.5	75.6	67.2	39.2	43.20	23.20	0.64	0.59
	2	123.3	89.6	53.2	64.20	36.10	0.72	0.68
	2.5	172.2	137.3	82.4	95.40	61.80	0.69	0.75
	3	224.4	182.4	106.4	121.20	75.80	0.66	0.71

Table 6. Backfill soil properties used in Finite element analysis

Description	**value**
Internal angle of friction, ϕ (°)	40.5°
Angle of dilation, ψ (°)	5°
Young's modulus, E_s (MPa)	70
Poisson's ratio, v	0.3
Mass Density, γ (kN/m^3)	19.72

Table 7. Comparison of the maximum surface heave radius for physical tests and numerical models, corresponding to a plate displacement of 20 mm

B (mm)	D/B	Maximum surface heave radius (cm)			
		Unreinforced		Reinforced	
		Test	Model	Test	Model
300	3	47.3	43.8	63.4	58.9
	2.5	42.4	40.8	59.3	55.7
	2	33.3	32.5	55.2	53.8
	1.5	32.8	32.4	52.1	51.7
225	3	37.2	34.8	49.1	49.6
	2.5	34.2	32.9	45.2	45.6
	2	29.4	28.6	43.3	44.6
	1.5	25.8	25.4	41.2	43.1
150	3	30.1	27.8	40.4	40.8
	2.5	27.3	25.2	38.2	39.3
	2	23.4	22.5	37.5	38.1